Joint profiling of proteins and DNA in single cells reveals extensive proteogenomic decoupling in leukemia

Benjamin Demaree[1,2,†], Cyrille L. Delley[1,†], Harish N. Vasudevan[1,3], Cheryl A.C. Peretz[4], David Ruff[5], Catherine C. Smith[4], Adam R. Abate[1,2,6,*]

[1]Department of Bioengineering and Therapeutic Sciences, University of California, San Francisco, San Francisco, California, USA
[2]UC Berkeley-UCSF Graduate Program in Bioengineering, University of California, San Francisco, California, USA
[3]Department of Radiation Oncology, University of California, San Francisco, California, USA
[4]Division of Hematology/Oncology, Department of Medicine, University of California, San Francisco, California, USA
[5]Mission Bio, Inc., San Francisco, California, USA
[6]Chan Zuckerberg Biohub, San Francisco, California, USA

*Corresponding author.
[†]These authors contributed equally to this work.

Correspondence to:
Adam R. Abate, Ph.D.
Department of Bioengineering and Therapeutic Sciences, University of California, San Francisco, 1700 4th St, San Francisco, California, USA; Email: adam@abatelab.org

Summary

Current leukemia therapies target cancer cells with specific phenotypes or genotypes, but this assumes that either genomic mutations or immunophenotypes alone serve as faithful proxies for treatment response[1]. Moreover, the heterogeneity inherent to all cancers, including leukemias, makes direct mapping of genotype-phenotype relationships challenging[2,3]. Here, we present a method to genotype and phenotype single cells at high throughput, allowing direct characterization of proteogenomic states on tens of thousands of cancer cells rapidly and cost efficiently. Using the approach, we analyze the disease of three leukemia patients over multiple treatment timepoints and recurrences. We observe complex genotype-phenotype dynamics and extensive decoupling of the relationships over disease progression and response to therapy, illustrating the subtlety of the disease process and the inability to use genotypes as direct proxies for phenotypes. Our technology has enabled the first rigorous test of the prevailing paradigm that treatment of a disease phenotype is equivalent to treatment of its underlying genotype. More broadly, our results highlight the power of single-cell multiomic measurements to resolve complex biology in heterogeneous populations, and illustrate how this information can be used to inform treatment. We thus expect that our methodology will find broad application to study proteogenomic tumor landscapes across cancers and will support the next generation of immunotherapy.

Main

Acute myeloid leukemia (AML) is an aggressive hematologic malignancy prone to relapse that often manifests as a polyclonal ensemble of cells with distinctive genotypes but diverse immunophenotypes[4,5]. Because of this disparity, it is difficult to directly link genotypes to immunophenotypes beyond circumstantial evidence from epidemiologic studies. Moreover, while AML blasts often exhibit immunophenotypes distinct from normal cells, with some surface markers even serving as therapeutic targets[6], genotypes are the strongest prognostic factors, suggesting a weak correspondence between these domains[7,8]. Cellular heterogeneity is an intrinsic aspect of essentially all cancers, including leukemias. Because cancer cells are heterogeneous in genotype and phenotype, single-cell analysis provides a powerful tool for characterizing this complexity and thereby advancing our understanding of different cancers. The value of single-cell analysis is its ability to correlate co-occurrence of different features in individual cells, with high-throughput technologies permitting analysis of thousands of cells to generate rich and intricate feature maps. For example, single-cell genotyping of AML-relevant loci has revealed co-occurrence of mutations and mapping of the clonal relationships between blasts[9–12]. These studies, however, have yet to map DNA genotypes and phenotypes in the same cells, precluding direct linkage of phenotypes to the genetic mutations that drive them.

To obtain simultaneous genotype and immunophenotype information, single cells can be sorted based on multi-parametric antibody analysis, and sequenced. While severely limited in throughput, these studies have uncovered important insights into the genetics of AML, identifying relevant aberrations such as single nucleotide polymorphisms (SNPs) and gene fusions[13]. Single-cell RNA sequencing (scRNA-seq) has emerged as a potentially valuable approach for genotype-phenotype linkage because it is cost effective and scalable[3,10,14,15]. The mRNA sequences provide genotype information[15,16] while their counts relate phenotype[17–21]. Moreover, modern approaches are extremely high throughput, allowing characterization of thousands of cells. Nevertheless, genotyping from mRNA remains a challenging and error-prone procedure that, even in the best case, provides incomplete information. For example, stochastic gene expression, biological biases[22], and limited coverage of essential genes combine to make assigning a genotype more difficult than can be achieved by direct analysis of DNA. Moreover, since RNA methods analyze only the expressed portion of the genome, mutations in intronic and other non-transcribed elements, like transcription factor binding sites, are omitted[23,24]. Thus, while several technologies have highlighted the importance of high-throughput single cell genotype-phenotype measurements, none provide the scalability and precision for comprehensive and accurate mapping of these clinically valuable biomarkers.

In this paper, we describe DAb-seq, a novel approach for joint profiling of DNA and surface proteins in single cells at high throughput. While existing methods attempt to obtain this information from the transcriptome alone, ours directly characterizes DNA for genotype and surface proteins for phenotype – both the gold standards in AML for these annotations. Our approach is thus complementary to scRNA-seq methods and, as we show, provides novel and important information for characterizing the disease. To illustrate the power of DAb-seq, we characterize the immunophenotypic and genotypic diversity underpinning AML in three patients at multiple timepoints, exploiting its throughput to characterize 50 DNA targets and 23 hematopoietic markers in a total of 54,717 cells. This analysis allows tracking of proteogenomic dynamics for multiple patients over multiple treatments and recurrences. We identify extensive genotype-phenotype decoupling, observing immunophenotypic heterogeneity among cells with a shared pathogenic mutation and genotypically diverse cells with a convergent malignant immunophenotype. These findings indicate substantial variability of blast fate upon treatment in AML, and that independent phenotype or genotype measurements do not adequately capture the proteogenomic heterogeneity. More broadly, our work demonstrates how single-cell technologies can inform the diagnosis and treatment of AML by elucidating the complex interplay between DNA mutations and their effects on protein expression.

Results

Combined single-cell DNA sequencing and antibody profiling (DAb-seq) robustly delineates single-cell genotypes and immunophenotypic diversity

The commercially available Mission Bio Tapestri supports highly multiplexed targeted sequencing of thousands of single cells and is being used across cancers for genotype and lineage mapping[11]. While the instrument runs a flexible workflow, it does not natively support Abseq, a separate method we developed[25] that allows characterization of single-cell surface proteins by sequencing, and is analogous to flow cytometry in its ability to provide immunophenotype information. Thus, our major technical innovation is to adapt Tapestri to enable simultaneous DNA and Abseq analysis. As in our published Abseq approach, DAb-seq begins with immunostaining of a cell suspension using a mixture of antibody-oligo conjugates (Figure 1A). Each antibody is associated with a known oligo tag; thus, when cells are stained with a pool of tagged antibodies, each cell is bound with a combination of antibodies and their tags based on surface protein profile. To characterize the profile, the tags must be sequenced and counted which, in flow cytometry, is analogous to measuring fluorescence of the dyes associated with each antibody, except that photon counting is replaced with tag counting.

The stained cells are processed through a modified Tapestri workflow to amplify and barcode genomic targets and surface-bound antibody tags. The workflow follows a two-step protocol to lyse cells and digest chromatin, making the genome accessible to amplification; the droplets are then subjected to a multiplex PCR to simultaneously amplify the genomic targets and capture antibody tags, labeling them with a droplet barcode relating sequences from the same cell (Figure 1B). For genotype, we target recurrently mutated genomic DNA loci in AML with primers containing a unique cell barcode against 50 amplicons spanning 19 genes. The primers and PCR conditions are tuned to enable uniform and quantitative amplification of all targets, since count information is necessary for accurate genotype and immunophenotype characterization. These primers also capture antibody tags from a 23-plex immunophenotyping panel based on those used in clinical minimal residual disease studies[26,27] (Figure 1C; Supplementary Table 3). Sequencing yields a multiomic data set where each cell is represented by two vectors and which can be visualized as a low-dimensional embedding (Figure 1D).

Peripheral blood mononuclear cells (PBMCs) comprise a diverse and well-understood population easily obtained from a blood draw, and thus provide an excellent sample by which to assess the effectiveness of DAb-seq for mapping hematopoietic immunophenotypes. When applied to PBMCs from a healthy donor, we obtain expected cell subsets across blood compartments, identifying both rare and abundant cells in peripheral blood (Figures 2A, 2B). To test single-cell genotyping capability, we also perform DAb-seq on a mixture of three cell lines derived from distinct hematopoietic lineages (Jurkat, Raji, K562) with documented mutations in the targeted genomic regions covered by our single-cell DNA sequencing panel[28] (Supplemental Table 2). For all genetic variants, we assign genotype calls to each individual cell: homozygous wildtype, heterozygous alternate, or homozygous alternate. We observe the expected correspondence between single-cell genotypes and phenotypes, as cells of the same genotype segregate within a common immunophenotypic cluster (Figures 2C, 2D). Notably, we also find that DAb-seq's genotyping is sufficiently sensitive to differentiate the cells based on zygosity of a given mutation (Figure 2D). These results show that DAb-seq can simultaneously profile genotype from direct analysis of genomic DNA and immunophenotype from barcoded antibodies.

NPM1-mutated cells persist across therapy timepoints with a static immunophenotype

AML therapies targeted to cell surface proteins require ubiquitous expression of the target marker on the malignant cells. We therefore reason that mutated cells should robustly associate with a common targeted phenotype in patients responsive to this therapy. To investigate this, we perform DAb-seq on 21,952 total cells from bone marrow aspirates of a patient with AML receiving gemtuzumab, a CD33-targeted therapy, across four treatment timepoints (Figure 3A). This patient received multiple rounds of chemotherapy, including a stem cell transplantation, prior to the first timepoint sampled in this study (Supplementary Table 1). In the single-cell DNA genotyping data, we identify a recurrent frameshift mutation in the *NPM1* gene (*NPM1*^{mut}) across relapse, salvage therapy, and progression timepoints. In addition, the *NPM1* mutation is found to always co-occur with a mutation at the *DNMT3A* locus (Figure 3A). Gemtuzumab targets CD33^{+} cells, which are extinguished at the remission timepoint[29]. To examine the immunophenotypic profile of the *NPM1*^{mut} blast population, we plot single-cell CD33 and CD34 values with *NPM1* mutation status across timepoints (Figure 3B). The proportion of *NPM1*^{mut} cells in the CD34^{-} and CD34^{+} compartments does not vary extensively across treatments, suggesting the lack of a therapeutic response in the blast immunophenotype. $CD33^+$ myeloid cells targeted by the drug are absent at remission.

In all timepoints for this patient, our analysis suggests an equivalence between the dominant blast genotype and corresponding phenotype. To further explore this relationship between genotype and phenotype, we visualize the high-dimensional single-cell immunophenotype as a Uniform Manifold Approximation and Projection[30] (UMAP) embedding of the antibody data (Figure 3C). Cells within single immunophenotypic clusters originate from different timepoints, highlighting the stability of normal and malignant immunophenotypes over time. When we overlay *NPM1* genotype on the immunophenotype UMAP space, we find a clear association between a single malignant immunophenotype composed of $CD33^+$ cells with *NPM1* mutation status, with variable expression of CD34, CD38, and CD117 in this population (Figure 3D). Indeed, this is in agreement with previous observations in flow cytometric studies where blast cells have been found to uniformly express CD33 and variably express CD34, CD38, and CD117[31]. Among the $NPM1^{wt}$ cells, we identify classical blood cell markers including CD3 and CD5 (lymphocyte), CD15 (monocyte), and CD56 (natural killer). Taken together, in this patient, DAb-seq confirms elimination of $CD33^+$ cells by gemtuzumab treatment and reveals a strong correspondence between genotype and phenotype across timepoints.

Genotypic subclones form overlapping subsets across an immunophenotypic continuum

To investigate whether such tight genotype-phenotype association is a universal feature of AML, we apply DAb-seq to a pediatric patient who underwent induction and consolidation chemotherapy, but ultimately relapsed (Supplementary Table 1). We identify two mutually exclusive *KRAS* and *FLT3*-mutated clones at diagnosis and relapse ($KRAS^{mut}$, $FLT3^{mut}$). The $FLT3^{mut}$ population, although the minor subclone at diagnosis comprising just 43 of 4,563 cells (0.94%) compared to 1,539 cells (33.7%) for the $KRAS^{mut}$ variant, dominates at relapse (6,800 of 7,516 cells, 90.5%) (Figure 4A). Immunophenotypically, we also identify a third subset comprising $KRAS^{WT}$/$FLT3^{WT}$ cells expressing a blast-like $CD33^+CD38^+$ immunophenotype with no identifiable DNA mutations in the targeted loci. When we group cells from all timepoints by genotype, pathogenic blasts display variable patterns in immunophenotype, with no clear mapping between the two (Figure 4B).

In the absence of an obvious genotype-phenotype mapping for this patient, we sought to investigate the underlying relationship between these domains. Using UMAP, we project the antibody data into two dimensions, coloring the points according to genotype (Figure 4C). We observe a single immunophenotypic compartment with incomplete separation between genotypes. To estimate antibody profile expression within the blast compartment continuum, we identify the dominant gradient in the phenotypic space, ordering all points along the gradient. We then calculate the local average antibody and genotypic composition for neighboring cells (Figure 4C, D) (Methods). As expected, many markers are anticorrelated (CD11b, CD33, CD56) or correlated (CD15) with the principal immunophenotypic gradient. Less trivially, genotypic compositions vary along the gradient, with $KRAS^{mut}$ clone frequencies anticorrelated and $FLT3^{mut}$ correlated (Figure 4D). Nevertheless, genotype composition never completely separates into individual clonal populations, making it impossible to define distinct genotype-phenotype clusters; consequently, technologies profiling one modality, such as genotyping or immunophenotyping, cannot adequately capture the heterogeneity inherent to this case of AML.

FLT3 inhibitor therapy induces erythroid differentiation in a case of AML

Our first two cases feature either a strong genotype-phenotype correlation (Patient 1) or mixed genotyping comprising a single immunophenotype (Patient 2). Thus, for our final case, we analyze a patient treated with gilteritinib, a FLT3 inhibitor therapy reported to promote *in vivo* differentiation of myeloid blasts. This treatment is thought to disperse distinct genotypes into multiple immunophenotypes, although the terminal lineage of the cells remains poorly understood[32–34]. Accordingly, we hypothesize DAb-seq should allow tracking of immunophenotypic dispersal and confirmation of their terminal hematopoietic lineage. We analyze 18,287 cells across treatment timepoints, beginning at diagnosis, discovering a subclone with co-mutated *DNMT3A* and *NPM1* (Figure 5A; Supplementary Table 1). Following cytarabine/daunorubicin induction therapy, a fraction of *DNMT3A^{mut}* cells remain at remission. At relapse and after treatment with the FLT3 inhibitor gilteritinib (“FLT3 Inhibitor”), most cells contain a 24-bp *FLT3* internal tandem duplication (ITD), in addition to the initial *DNMT3A* and *NPM1* mutations. The genotypic structure inferred from the single-cell data indicates a linear, branching hierarchy of sequentially acquired mutations in response to therapy. To explore the immunophenotypic features of this patient’s disease, we integrate cells from all timepoints and construct a UMAP representation using the antibody data (Figure 5B). We cluster this data using the Leiden method for cluster detection, an improved algorithm over Louvain modularity[35,36], and manually annotate with phenotypic labels corresponding to hematopoietic lineage from the antibody data (Figure 5C). We identify three blast populations expressing high levels of CD33 and CD38, a monocytic population expressing CD15 and CD16, and erythroid and lymphoid clusters with elevated CD71 and CD3. As expected, samples across treatment timepoints comprise a mixture of immunophenotypically normal and blast-like cells.

Hypothesizing that different therapies should yield different genotype-phenotype coupling patterns, we sought to characterize how mutated and normal cells distribute across immunophenotypic clusters. For each timepoint, we thus label cells in UMAP space according to DNA genotype and generate density distributions of CD33 signal, a pan-myeloid marker (Figure 5D). We also evaluate counts of phenotype cluster membership in each timepoint, subdivided by DNA genotype. At diagnosis, cells mutated at both the *DNMT3A* and *NPM1* locus reside primarily in the Blast 1 cluster (81.8% of *DNMT3A^{mut}/NPM1^{mut}* cells) and express high levels of CD33. A secondary clone mutated exclusively at the *DNMT3A* locus exhibits comparable CD33 expression and resides mainly in the Blast 1 and monocytic clusters (62.5% and 27.7% of *DNMT3A^{mut}* cells, respectively). At remission, the same *DNMT3A^{mut}* clone is identified but with decreased CD33 expression and a primarily monocytic immunophenotype (92.7% of *DNMT3A^{mut}* cells) co-localizes with cells of normal genotype, consistent with clonal hematopoiesis of a pre-leukemic clone[37,38]. A newly acquired *FLT3*-ITD clone emerges in high numbers at relapse (99.8% of genotyped cells), coinciding with a phenotypic shift of cells to the CD33^{+} Blast 2 cluster. Following FLT3 inhibitor treatment, the same *FLT3*-ITD clone persists but exhibits a transformed immunophenotype, as evidenced by membership of the *FLT3* clone in multiple immunophenotypic clusters. The new *FLT3*-ITD immunophenotype is primarily erythroid (82.2% of *FLT3*-ITD cells), with minor fractions in the Blast 3 and monocytic compartments (11.1% and 4.84% of *FLT3*-ITD cells, respectively). Furthermore, the *FLT3*-ITD clone at relapse lacks uniform CD33 expression, indicating that this clone is no longer restricted to the myeloid compartment. Taken together, these findings support the model of terminal erythroid differentiation of blasts in a case of leukemia treated with gilteritinib. In agreement with a recent study[34], proteogenomic analysis by DAb-seq challenges a prior report of gilteritinib-induced terminal differentiation towards a myeloid fate[33]. DAb-seq elucidates the rich and complex dynamics of this process and illustrates how distinct DNA genotypes can fractionate into multiple phenotypic identities in response to treatment.

Discussion

Through its ability to jointly profile DNA and immunophenotype, DAb-seq captures the complexity of proteogenomic states underlying AML. Analysis of multiple patients over timepoints and treatments demonstrates the plasticity of the disease and the complex and unpredictable way it progresses in different contexts. In a patient with extensive clinical history including multiple rounds of chemotherapy, we found a robust relationship between mutant *NPM1* cells and a malignant phenotype; this suggested that a single CD33-targeted therapy would eradicate the blast population, as indeed it did. By contrast, in a separate case of pediatric AML, we observed that genetically distinct populations shared overlapping immunophenotype, demonstrating that this domain alone is insufficient for characterizing how cells are genetically programmed and may, consequently, respond to treatment. In the final case study, we observed the opposite scenario, in which treatment by gilteritinib induced mutationally similar cells to disperse into different myeloid compartments, highlighting the challenge of targeting these malignant cells for eradication. Our results thus demonstrate that genotype or immunophenotype alone is insufficient to predict the evolution of proteogenomic states in AML.

DAb-seq employs targeted primers to amplify specific genomic regions and panels of antibodies. While both readouts enable massive multiplexing of queried targets, practical and economic constraints necessitate *a priori* knowledge of which loci and epitopes to profile. As such, the strength of DAb-seq is not unbiased feature discovery, as with scRNA-seq, but rather sensitive and precision analysis of actionable information. Furthermore, as with all targeted methods of DNA genotyping, DAb-seq cannot exclude the possibility that disease-relevant mutations occur beyond the sequenced loci or in immunophenotypic markers not included in the panels. In the case of pediatric AML, it is therefore impossible for us to conclude if the *FLT3*^{wt}/*KRAS*^{wt} blast population is driven by epigenetic changes or unmapped genomic aberrations. Nevertheless, the sensitivity of DAb-seq, and its low genotyping drop-out, allows identification of co-occurring mutations, including heterozygous mutations that are notoriously difficult for RNA-based approaches. Moreover, DAb-seq firmly places genomic mutations in understood phenotypic contexts, which is vital for understanding how they program the disease and, ultimately, treatments select for them.

In the era of personalized medicine, treatment decisions are increasingly based on DNA mutation status, such as targeted EGFR inhibitors or protein expression like HER2 or PD-L1 status. To fully leverage the capabilities of modern profiling techniques, however, information across all available domains must be integrated to optimize the therapeutic strategy for a given patient. Indeed, our findings underscore the importance of utilizing both genotype and immunophenotype to fully characterize disease and assess efficacy of treatment. For example, CAR T-cell therapy derives specificity from protein expression, yet would fail to elicit a complete response if pathogenic genotypes were distributed across multiple phenotypic clusters. Such a scenario would require joint single-cell profiling as in DAb-seq to unravel. As multiomic single-cell technologies like DAb-seq become available, it will be feasible to use comprehensive precision analysis to deconvolute the subtlety of each patient's cancer and thereby select the best treatment regimen.

Methods

Conjugation of antibodies to oligonucleotide barcodes

Monoclonal antibodies were conjugated to azide-modified oligonucleotides using a copper-free click chemistry reaction as described previously[39]. Monoclonal antibodies were resuspended to 100 µg in 100 µL PBS. See Supplementary Table 3 for a complete list of antibodies and oligonucleotide barcode sequences. Antibodies were incubated with DBCO-PEG5-NHS Ester linker (Click Chemistry Tools, cat. no. A102P) at a 4:1 molar ratio linker:antibody for 2 h at room temperature. Following incubation, the antibody-linker solution was washed once in a 50 kDa cellulose spin filter (Millipore Sigma, cat. no. UFC505024). DNA oligonucleotides with a 5' azide modification (Integrated DNA Technologies) were reconstituted in water and added to the washed antibodies at a 2.5:1 molar ratio oligonucleotide:antibody. Following a 16 h incubation, the conjugated antibodies were washed three times in a 50 kDa filter to remove unreacted oligonucleotides. All antibody conjugates were run on a Bioanalyzer Protein 230 electrophoresis chip (Agilent Technologies, cat. no. 5067-1517) to verify successful conjugation.

Cell culture and PBMC processing for control experiments

The following three cell lines were used in the initial control experiment: Raji (ATCC, CCL-86), Jurkat (ATCC, TIB-152), K562 (ATCC, CCL-243). Cells were cultured under the supplier's recommended conditions. PBMCs from a single healthy donor were sourced commercially (iXCells Biotechnologies, cat. no. 10HU-003) and stored at -80°C until use. Prior to staining, the cultured cell lines and PBMCs were washed once in PBS with 5% fetal bovine serum (FBS) (Thermo Fisher, cat. no. 10082147). For the control experiment, the three cell lines were combined at an equal ratio.

Collection of patient samples

Patients included in this study were treated at the University of California, San Francisco (UCSF), and peripheral blood or bone marrow was stored in the UCSF tumor bank. Samples were processed immediately after collection to isolate mononuclear cells. Sample collection was in accordance with the Declaration of Helsinki under institutional review board-approved tissue banking protocols. Written informed consent was obtained from all patients.

Thawing patient samples

A protocol was optimized to maximize recovery of viable cells from patient samples. Cryovials containing patient tissue (peripheral blood or bone marrow aspirate) were warmed by hand and carefully transferred dropwise to a 50 mL tube containing 40 mL of cold DMEM media (Thermo Fisher, cat. no. 11995040) with 20% FBS and 2 mM EDTA. The tube was centrifuged at 700 rpm at 4°C for 7 min with no brake. The supernatant was discarded, and the cells were resuspended in

10 mL of warmed RPMI-1640 media (Thermo Fisher, cat. no. A1049101) with 10% FBS. The solution was strained through a 70 μm cell strainer (Corning, cat. no. 431751) to remove any large cell aggregates and the tube was centrifuged a second time at 700 rpm at 4°C for 5 min with low brake. The supernatant was discarded, and the cells were resuspended in PBS with 5% FBS for staining.

Cell staining using oligonucleotide-conjugated antibodies

For each sample, 2 million cells were added to a 5 mL DNA LoBind tube (Eppendorf, cat. no. 0030108310), centrifuged at 400 x g for 4 min, and resuspended in 180 μL PBS with 5% FBS. Cells were blocked for 10 min on ice following addition of 10 μL Fc blocking solution (BioLegend, cat. no. 422301), 4 μL of a 1% dextran sulfate solution (Research Products International, cat. no. D20020), and 4 μL of 10 mg/mL salmon sperm DNA (Invitrogen, cat. no. 15632011). Cells were stained for 30 min on ice with 0.5 μg of each conjugated antibody. After incubation, five rounds of washing were performed to remove excess antibody. For each wash, 5 mL PBS with 5% FBS was added to the tube and centrifuged at 400 x g for 4 min. Stained cells were resuspended in Mission Bio cell buffer at a final concentration of 3 M/mL prior to microfluidic encapsulation.

Microfluidic single-cell DNA genotyping and antibody capture

A commercial single-cell DNA genotyping platform (Mission Bio, Tapestri) was used to perform microfluidic encapsulation, lysis, and barcoding according to the manufacturer's protocol for the acute myeloid leukemia V1 panel. Where noted, modifications were made to enable co-capture of oligonucleotide-labeled antibodies. Stained cells were loaded into a microfluidic cartridge and co-encapsulated into droplets with a lysis buffer containing protease and mild detergent. Droplets were incubated in a thermal cycler for 1 h at 50°C to digest all cellular proteins, followed by 10 min at 80°C to heat-inactivate the protease. To enable antibody capture during the barcoding stage, the antibody tags were designed with 3' complementarity to one of the *RUNX1* gene forward primers and the corresponding reverse primer was omitted from the reverse primer pool. Supplementary Table 2 lists the sequences of the forward and reverse primers in the DNA panel. Lysed cells in droplets were transferred to the barcoding module of the microfluidic cartridge in addition to polymerase mix, the modified reverse primer pool, barcoded hydrogel beads, and oil for droplet generation. The droplets were placed under a UV lamp (Analytik Jena, Blak-Ray XX15L) for 8 min to cleave the single-stranded PCR primers containing unique cell barcodes from the hydrogel beads. To amplify DNA targets and capture antibody tags, droplets were thermal cycled using the following program: 95°C for 10 m; 20 cycles of (95°C for 30 s, 72°C for 10 s, 61°C for 4 min, 72°C for 30 s); 72°C for 2 min; 4°C hold.

Single-cell DNA amplicon and antibody tag sequencing library preparation

Recovery and cleanup of single-cell libraries proceeded according to the Mission Bio V1 protocol with additional modifications for antibody library preparation. The 8 PCR tubes containing barcoded droplets were pooled as pairs and treated with Mission Bio Extraction Agent. Water was added to each tube and the aqueous fraction transferred to a new 1.5 mL DNA LoBind tube. Ampure XP beads (Beckman Coulter, cat. no. A63881) were added at a 0.75X volume ratio beads:PCR product for size selection. The supernatant from the size selection step, containing library fragments shorter than ~200 bp, was retained and used for antibody library preparation, while the remaining beads with bound DNA panel library fragments were washed twice with 80% EtOH and eluted in 30 μL water. A biotinylated capture oligonucleotide

(/5Biosg/GGCTTGTTGTGATTCGACGA/3C6/, Integrated DNA Technologies) complementary to the 5' end of the antibody tags was added to the retained supernatant to a final concentration of 0.6 µM. The supernatant-probe solution was heated to 95°C for 5 min to denature the PCR product, then snap-cooled on ice for probe hybridization. 10 µL of streptavidin beads (Thermo Fisher, cat. no. 65001) were washed according to the manufacturer's protocol and added to each tube of PCR product. Following a 15 min incubation at room temperature, the beads were isolated by magnetic separation, washed two times in PBS, and resuspended in 30 µL water. PCR was performed on the purified DNA panel and antibody tags to produce sequencing libraries. For each tube of purified DNA panel, 50 µL reactions were prepared containing 4 ng of barcoded product in 15 µL water, 25 µL Mission Bio Library Mix, and 5 µL each of custom P5 and Nextera P7 primers (N7XX), both at 4 µM stock concentration. The reactions were thermal cycled using the following program: 95°C for 3 min; 10 cycles of (98°C for 20 s, 62°C for 20 s, 72°C for 45 s); 72°C for 2 min; 4°C hold. For each tube of purified antibody tags, identical reactions were prepared, instead using 15 µL bead-bound template, 5 µL antibody tag-specific P7 primer at 4 µM, and 20 cycles of amplification. See Supplementary Table 4 for a complete listing of custom library preparation primers. Following amplification, both the DNA panel and antibody tag libraries were cleaned with 0.7X Ampure XP beads and eluted in 12 µL water.

Next-generation sequencing

All DNA panel and antibody tag libraries were run on a Bioanalyzer High Sensitivity DNA electrophoresis chip (Agilent Technologies, cat. no. 5067-4626) to verify complete removal of primer-dimer products. Libraries were quantified by fluorometer (Qubit 3.0, Invitrogen) and sequenced on Illumina next-generation sequencing platforms with a 20% spike-in of PhiX control DNA (Illumina, cat. no. FC-110-3001). All sequencing runs used a dual-index configuration and a custom Read 1 primer (5' GCCTGTCCGCGGAAGCAGTGGTATCAACGCAGAGTAG 3', Integrated DNA Technologies). The 3-cell control sample was sequenced on an Illumina MiSeq using a v2 300-cycle kit in 2x150 bp paired-end mode (Illumina, cat. no. MS-102-2002). For the patient samples, DNA panel and antibody tag libraries were sequenced separately to maximize cost-effectiveness. DNA panels were sequenced with an Illumina NovaSeq 6000 SP 300-cycle Kit (Illumina, cat. no. 20027465) in 2 x 150 bp paired-end mode. Antibody tag libraries were sequenced with an Illumina NextSeq 550 75-cycle High Output Kit (Illumina, cat. no. 20024906) in paired-end mode, using 38 cycles for Read 1 and 39 cycles for Read 2.

Bioinformatic pipeline for single-cell DNA genotyping and antibody tag counting

Sequencing data was processed using a custom pipeline available on GitHub (see Code Availability). For all reads, combinatorial cell barcodes were parsed from Read 1 using cutadapt (v2.4) and matched to a barcode whitelist. Barcode sequences within a Hamming distance of 1 from a whitelist barcode were corrected.

For the DNA genotyping libraries, reads with valid barcodes were trimmed with cutadapt to remove 5' and 3' adapter sequences and demultiplexed into single-cell FASTQ files using the script "demuxbyname" from the BBMap package (v.38.57). Valid cell barcodes were selected using the inflection point of the cell rank plot in addition to the requirement that 60% of DNA intervals were covered by a minimum of 8 reads. FASTQ files for valid cells were aligned to the hg19 build of the human genome reference using bowtie2 (v2.3.4.1). The single-cell alignments in BAM format were filtered (properly mapped, mapping quality > 2, primary alignment), sorted, and indexed with samtools (v1.8). GVCF files were produced for all cells using HaplotypeCaller from the GATK suite (v.4.1.3.0). Joint genotyping was performed on all genomic intervals in parallel (excluding primer regions) using GATK GenotypeGVCFs. For longitudinal patient samples, cells from all timepoints were joint genotyped as a multi-sample cohort. Genotyped intervals from all cells were combined into a single variant call format (VCF) file, and multiallelic records were split and left-aligned using bcftools (v1.9). Variants were annotated with ClinVar metadata (v.20190805) and SnpEff functional impact predictions (v4.3t). Variant records for all cells were exported to HDF5 format using a condensed representation of the genotyping calls (0: wildtype; 1: heterozygous alternate; 2: homozygous alternate; 3: no call).

The antibody tag libraries were processed identically for cell barcode demultiplexing. For reads with valid cell barcodes, 8 bp antibody barcodes and 10 bp unique molecular identifiers (UMIs) were extracted from Read 2 using cutadapt with the requirement that all UMI bases had a minimum quality score of 20. Antibody barcode sequences within a Hamming distance of 1 from known antibody barcodes were corrected. UMI sequences were grouped by cell and antibody and counted using the UMI-tools package (v.0.5.3, “adjacency” method). UMI counts of antibodies for each cell barcode were exported in tabular format for further analysis.

Cell and genotype filtering

Cell barcodes were additionally filtered according to antibody counts. Valid barcode groups were required to have a minimum of 100 antibody UMIs by the adjacency counting method and a maximum IgG1 count no greater than five times the median IgG1 count of the associated DAb-seq experiment. For each valid cell barcode, all variants were filtered according to the quality and sequence depth reported by GATK. Genotyping calls were required to have a minimum quality of 30 and total depth of 10; variant entries below these thresholds were marked as “no call” and excluded from analyses.

Antibody-based embedding and clustering

To correct for technical effects in the raw antibody counts and batch variability between experiments from the same patient but different time points, a linear regression over all cells from the same patient was performed. Specifically, to all entries $\mathbf{c}_{ij}$ of the UMI corrected antibody count matrix $\mathbf{c}$, where i is the cell index and j the antibody index, one pseudocount was added and the matrix was log-transformed. A matrix of quality metrics $\mathbf{q}$ with cells as rows and four columns (total antibody reads, total antibody counts after UMI correction, IgG1 count and total amplicon reads) was log-transformed, column-wise normalized, and mean-centered. A singular value decomposition was performed on the transformed matrix $\mathbf{q}$ and the left-singular vectors retained as design matrix. Each column vector $\mathbf{c}_j$ was then regressed with either the first three, two, or one left-singular vectors, for patient samples, PMBC or cell lines respectively as regressors. The vector of residuals $\mathbf{u}_j$ is then the corrected antibody signal of antibody j (Extended Data Figure 1).

A UMAP embedding in two dimensions of the corrected antibody signal was done in Python 2.7 using the umap-learn[30] (v0.3.10) and scanpy[40] (v.1.4.4.post1) packages, with the minimum distance parameter set to 0.1 for the pediatric patient and 0.2 for all other samples and default parameters otherwise. To construct the underlying nearest neighbor graph from the corrected antibody count matrix, 15 or 16 nearest neighbors based on the first 16 to all principal components were used. The scanpy implementation of the Leiden algorithm[35] with resolution set to 0.1 for the three cell line experiment and 1 otherwise was used to assign cells to phenotypic compartments. For the gradient analysis of the pediatric Patient with AML (Figure 4), only cells belonging to Leiden communities with blast phenotype were retained and the singular value decomposition of the remaining rows of **u** was calculated. Cells were then ordered by their value of the second left-singular vector. Antibody counts and genotype fractions along the gradient were averaged with a moving window of 200 cells. Similarly, the average position of the cells in the two-dimensional UMAP embedding was estimated by smoothing x and y coordinates with a moving window of the same length. A 3rd-order spline was placed through the smoothed cell position to indicate the orientation of the gradient in the UMAP embedding.

Code Availability

The DAb-seq bioinformatic pipeline will be available on GitHub at https://github.com/AbateLab/DAb-seq upon final publication.

Data Availability

All sequencing data generated in this study will be available on the Sequence Read Archive under BioProject number PRJNA602320 upon final publication.

Acknowledgments

This work was supported by the Chan Zuckerberg Biohub, the National Science Foundation CAREER Award (Award Number DBI-1253293), and the National Institutes of Health (Award Numbers 2R01EB019453 and 1DP2AR068129). C.L.D. is supported by a Swiss National Science Foundation fellowship (Grant No. 183853). C.A.C.P. is supported by Alex's Lemonade Stand Young Investigator Award, the Conquer Cancer ASCO Young Investigator Award, and by the National Center for Advancing Translational Sciences of the NIH under Award Number (TBD). C.C.S. is supported by a Research Scholar Award from the American Cancer Society and is the Damon Runyon-Richard Lumsden Foundation Clinical Investigator supported (in part) by the Damon Runyon Cancer Research Foundation (CI-99-18). Research contents are solely the responsibility of the authors and do not necessarily represent the official views of the NIH. We thank Aik Ooi at Mission Bio for his help with antibody conjugations and Mission Bio for donating reagents.

Author Contributions

B.D. and C.L.D. performed the experiments, sequenced the samples, analyzed the data, and wrote the initial draft of the manuscript. C.A.C.P. assisted with patient sample processing. H.N.V. and A.A. revised the manuscript. C.S. treated the patients and obtained samples. All authors read, reviewed, and approved the manuscript.

References

1. Arber, D. A. *et al.* The 2016 revision to the World Health Organization classification of

myeloid neoplasms and acute leukemia. *Blood* **127**, 2391–2405 (2016).

2. Marusyk, A., Almendro, V. & Polyak, K. Intra-tumour heterogeneity: a looking glass for cancer? *Nat. Publ. Gr.* **12**, 323–334 (2012).
3. Suvà, M. L. & Tirosh, I. Single-Cell RNA Sequencing in Cancer: Lessons Learned and Emerging Challenges. *Mol. Cell* **75**, 7–12 (2019).
4. Landau, D. A., Carter, S. L., Getz, G. & Wu, C. J. Clonal evolution in hematological malignancies and therapeutic implications. *Leukemia* **28**, 34–43 (2014).
5. Patel, J. P. *et al.* Prognostic Relevance of Integrated Genetic Profiling in Acute Myeloid Leukemia. *N. Engl. J. Med.* **366**, 1079–1089 (2012).
6. Buckley, S. A. & Walter, R. B. Antigen-specific immunotherapies for acute myeloid leukemia. *Hematology* **2015**, 584–595 (2015).
7. García-Dabrio, M. C. *et al.* Complex Measurements May Be Required to Establish the Prognostic Impact of Immunophenotypic Markers in AML. *Am. J. Clin. Pathol.* **144**, 484–492 (2015).
8. Papaemmanuil, E. *et al.* Genomic Classification and Prognosis in Acute Myeloid Leukemia. *N. Engl. J. Med.* **374**, 2209–2221 (2016).
9. Paguirigan, A. L. *et al.* Single-cell genotyping demonstrates complex clonal diversity in acute myeloid leukemia. *Sci. Transl. Med.* **7**, 281re2 (2015).
10. Wang, L. *et al.* Integrated single-cell genetic and transcriptional analysis suggests novel drivers of chronic lymphocytic leukemia. *Genome Res.* **27**, 1300–1311 (2017).
11. Pellegrino, M. *et al.* High-throughput single-cell DNA sequencing of acute myeloid leukemia tumors with droplet microfluidics. *Genome Res.* **28**, 1345–1352 (2018).
12. Smith, C. C. *et al.* Heterogeneous resistance to quizartinib in acute myeloid leukemia revealed by single-cell analysis. *Blood* **130**, 48–58 (2017).
13. De Zen, L. *et al.* Quantitative multiparametric immunophenotyping in acute lymphoblastic leukemia: correlation with specific genotype. I. ETV6/AML1 ALLs identification. *Leukemia* **14**, 1225–1231 (2000).
14. van Galen, P. *et al.* Single-Cell RNA-Seq Reveals AML Hierarchies Relevant to Disease Progression and Immunity. *Cell* **0**, 1–17 (2019).
15. Giustacchini, A. *et al.* Single-cell transcriptomics uncovers distinct molecular signatures of stem cells in chronic myeloid leukemia. *Nat. Med.* **23**, 692–702 (2017).
16. Nam, A. S. *et al.* Somatic mutations and cell identity linked by Genotyping of Transcriptomes. *Nature* **571**, 355–360 (2019).
17. Shalek, A. K. *et al.* Single-cell transcriptomics reveals bimodality in expression and splicing in immune cells. *Nature* **498**, 236–240 (2013).
18. Macosko, E. Z. *et al.* Highly Parallel Genome-wide Expression Profiling of Individual Cells Using Nanoliter Droplets. *Cell* **161**, 1202–1214 (2015).
19. Klein, A. M. *et al.* Droplet Barcoding for Single-Cell Transcriptomics Applied to Embryonic Stem Cells. *Cell* **161**, 1187–1201 (2015).
20. Zeisel, A. *et al.* Brain structure. Cell types in the mouse cortex and hippocampus revealed by single-cell RNA-seq. *Science* **347**, 1138–42 (2015).
21. Schiebinger, G. *et al.* Optimal-Transport Analysis of Single-Cell Gene Expression Identifies Developmental Trajectories in Reprogramming. *Cell* **176**, 928-943.e22 (2019).
22. Deng, Q., Ramsköld, D., Reinius, B. & Sandberg, R. Single-cell RNA-seq reveals dynamic, random monoallelic gene expression in mammalian cells. *Science (80-.).* **343**, 193–196 (2014).

23. Mansour, M. R. *et al.* Oncogene regulation. An oncogenic super-enhancer formed through somatic mutation of a noncoding intergenic element. *Science* **346**, 1373–7 (2014).

24. Rheinbay, E. *et al.* Analyses of non-coding somatic drivers in 2,658 cancer whole genomes. *Nature* **578**, 102–111 (2020).

25. Shahi, P., Kim, S. C., Haliburton, J. R., Gartner, Z. J. & Abate, A. R. Abseq: Ultrahigh-throughput single cell protein profiling with droplet microfluidic barcoding. *Sci. Rep.* **7**, 1–12 (2017).

26. Schuurhuis, G. J. *et al.* Minimal/measurable residual disease in AML: a consensus document from the European LeukemiaNet MRD Working Party. *Blood* **131**, 1275–1291 (2018).

27. Wood, B. L. Flow Cytometric Monitoring of Residual Disease in Acute Leukemia. in 123–136 (Humana Press, Totowa, NJ, 2013). doi:10.1007/978-1-62703-357-2_8

28. Tate, J. G. *et al.* COSMIC: the Catalogue Of Somatic Mutations In Cancer. *Nucleic Acids Res.* **47**, D941–D947 (2019).

29. Appelbaum, F. R. & Bernstein, I. D. Gemtuzumab ozogamicin for acute myeloid leukemia. *Blood* **130**, 2373–2376 (2017).

30. McInnes, L., Healy, J. & Melville, J. UMAP: Uniform Manifold Approximation and Projection for Dimension Reduction. (2018).

31. Campana, D. & Behm, F. G. Immunophenotyping of leukemia. *J. Immunol. Methods* **243**, 59–75 (2000).

32. Sexauer, A. *et al.* Terminal myeloid differentiation in vivo is induced by FLT3 inhibition in FLT3/ITDAML. *Blood* **120**, 4205–4214 (2012).

33. McMahon, C. M. *et al.* Gilteritinib induces differentiation in relapsed and refractory FLT3-mutated acute myeloid leukemia. *Blood Adv.* **3**, 1581–1585 (2019).

34. Yun, H. D. *et al.* Erythroid differentiation of myeloblast induced by gilteritinib in relapsed FLT3-ITD–positive acute myeloid leukemia. *Blood Advances* **3**, 3709–3712 (2019).

35. Traag, V. A., Waltman, L. & van Eck, N. J. From Louvain to Leiden: guaranteeing well-connected communities. *Sci. Rep.* **9**, 5233 (2019).

36. Blondel, V. D., Guillaume, J.-L., Lambiotte, R. & Lefebvre, E. Fast unfolding of communities in large networks. (2008). doi:10.1088/1742-5468/2008/10/P10008

37. Buscarlet, M. *et al.* DNMT3A and TET2 dominate clonal hematopoiesis and demonstrate benign phenotypes and different genetic predispositions. *Blood* **130**, 753–762 (2017).

38. Jaiswal, S. *et al.* Clonal Hematopoiesis and Risk of Atherosclerotic Cardiovascular Disease. *N. Engl. J. Med.* **377**, 111–121 (2017).

39. Gong, H. *et al.* Simple Method To Prepare Oligonucleotide-Conjugated Antibodies and Its Application in Multiplex Protein Detection in Single Cells. *Bioconjug. Chem.* **27**, 217–225 (2016).

40. Wolf, F. A., Angerer, P. & Theis, F. J. SCANPY: large-scale single-cell gene expression data analysis. *Genome Biol.* **19**, 15 (2018).

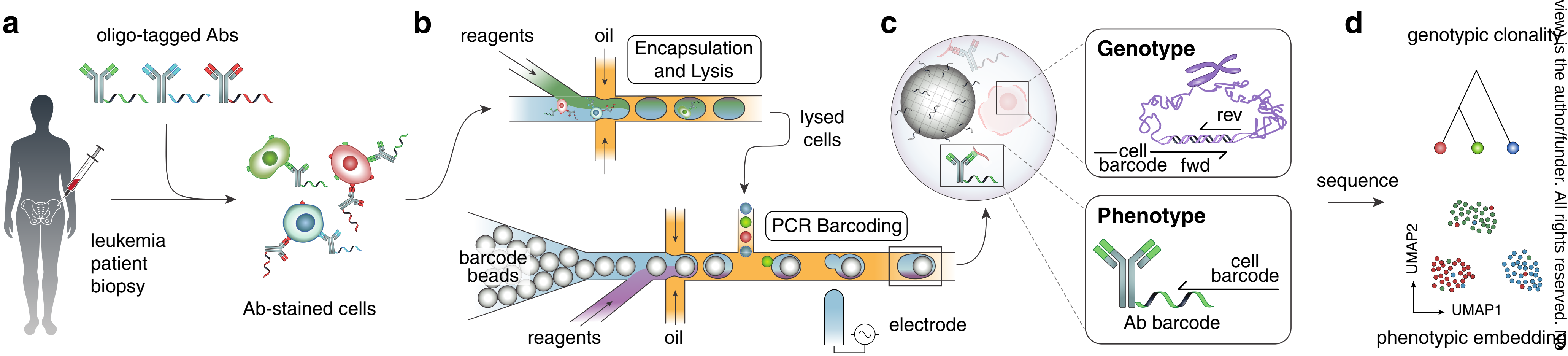

Figure 1: The DAb-seq workflow.
a, Bone marrow aspirates of patients with AML contain healthy and malignant cells that exhibit diverse genotypes and immunophenotypes. These cells are stained with antibodies labeled with DNA tags. **b**, Stained cells are paired and encapsulated with a barcode bead on a Mission Bio Tapestri instrument. **c**, In each droplet, a PCR labels antibody tags and genomic DNA targets simultaneously with a unique cell index. **d**, Sequencing the barcoded amplicons and antibody tags yields coupled single-cell immunophenotype and genotype data for thousands of cells.

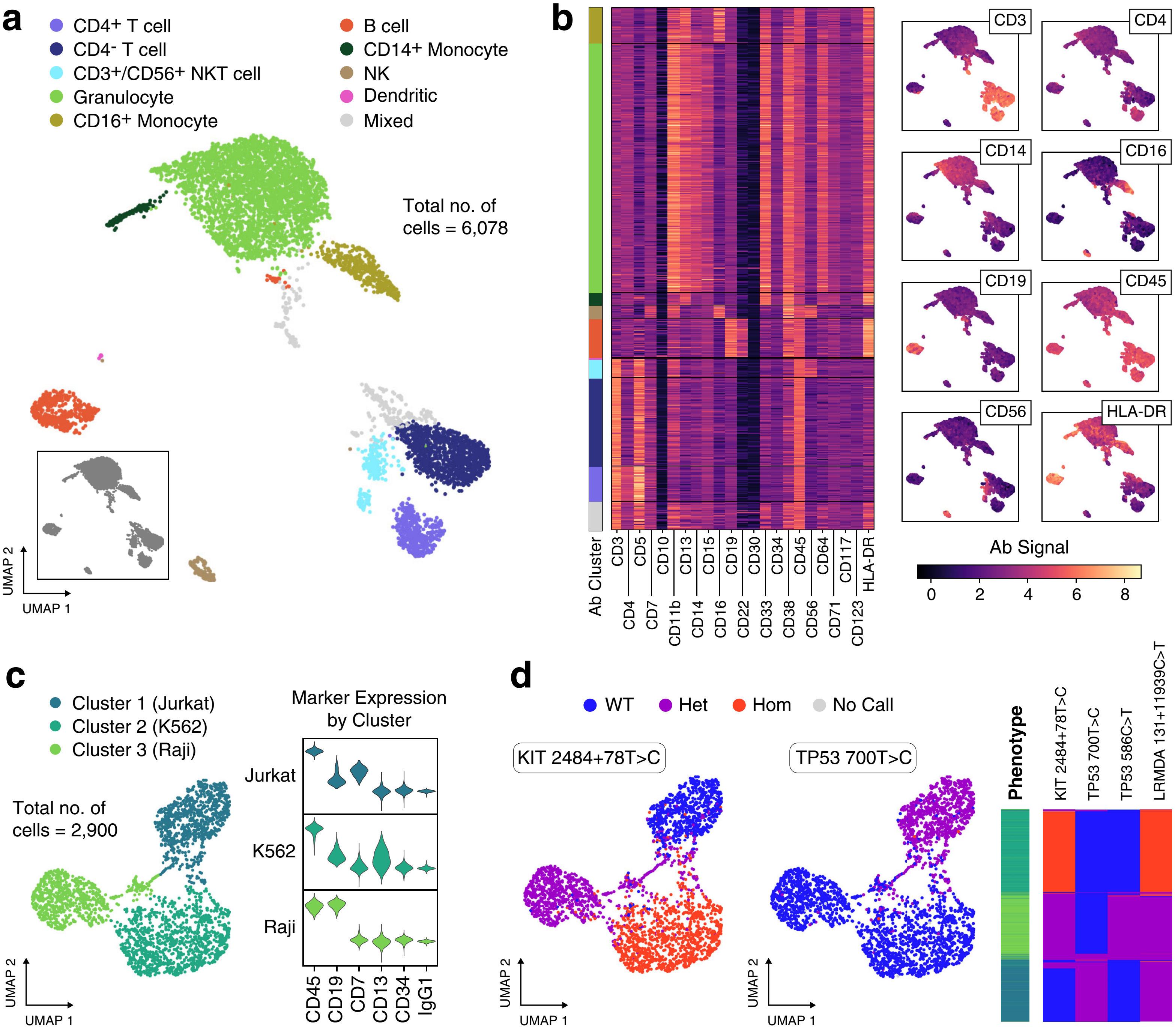

Figure 2: DAb-seq enables simultaneous discrimination of single cells by their immunophenotype and genotype. **a**, DAb-seq workflow performed on PBMCs from a healthy donor using a panel of 23 antibodies. Leiden clustering and two-dimensional UMAP embedding of the antibody tag data reveals expected blood compartments. Compartments are annotated based on detected marker expression. **b**, Heatmap of the corrected log-transformed antibody counts for each cell and antibody. Cells are ordered based on Leiden clusters. Overlay of corrected log-transformed antibody counts with the UMAP embedding highlights compartment-specific expression. **c**, Correspondence of antibody signal with genomic polymorphisms in DAb-seq experiments tested on a mixture of three cell lines and a panel of six antibodies. Cells cluster by antibody signal as shown in the UMAP embedding. **d**, Detected single nucleotide polymorphisms in these cells map to the phenotypic cell clusters as shown in the UMAP embedding and a heatmap, where rows correspond to single cells. The first column of the heatmap indicates assigned phenotype cluster, and the remaining columns indicate the genotyping call at the labeled loci.

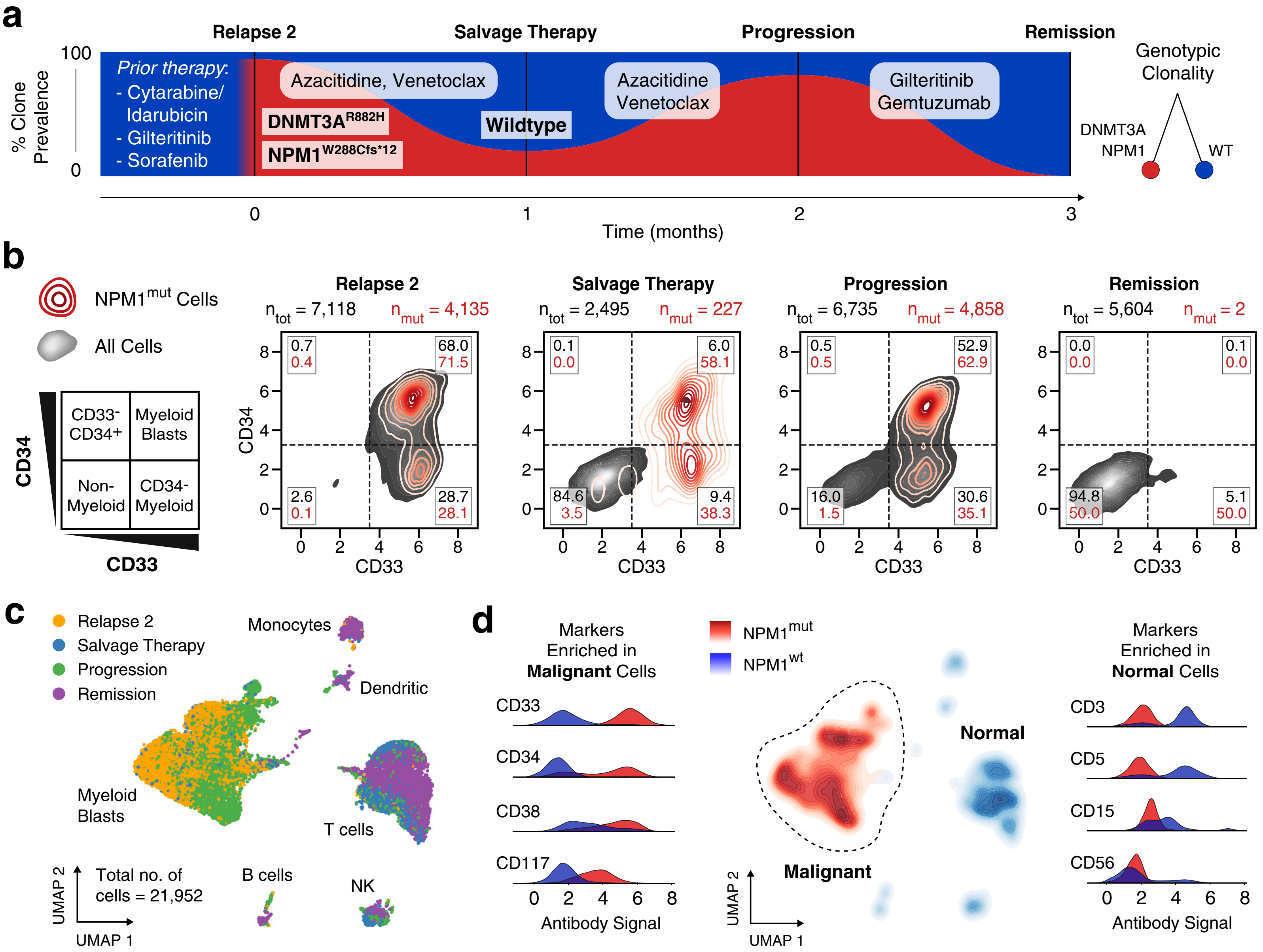

Figure 3: AML blasts exhibit a stable genotype and phenotype through treatment.
a, DAb-seq performed on four bone marrow aspirates of a patient with AML during disease progression as indicated in the fishplot (black lines). The patient received multiple rounds of chemotherapy prior to the experiment (Supplementary Table 1). The fraction of blast cells with NPM1 W288Cfs*12 (NPM1mut) mutation for each sampled time point detected by DAb-seq are shown in red. **b**, Scatter plots with kernel densities show CD33 and CD34 signal for all cells (grey) and NPM1mut cells (red) for each of the sampled time points. The percentage of normal and mutant cells within each gate are listed. Virtually gating cells highlights a persisting CD33+ blast population which is eradicated with gemtuzumab, a CD33-targeted therapy. **c**, UMAP embedding based on the log-transformed and corrected antibody counts from all cells labeled by timepoint indicates that the high-dimensional immunophenotype of the blasts is stable over the sampled timepoints. **d**, The genotype of each cell at the NPM1 locus is plotted as a kernel density estimate using the UMAP coordinates from c. Antibody signals enriched among malignant and normal populations are plotted as kernel densities using all cells and labeled by genotype.

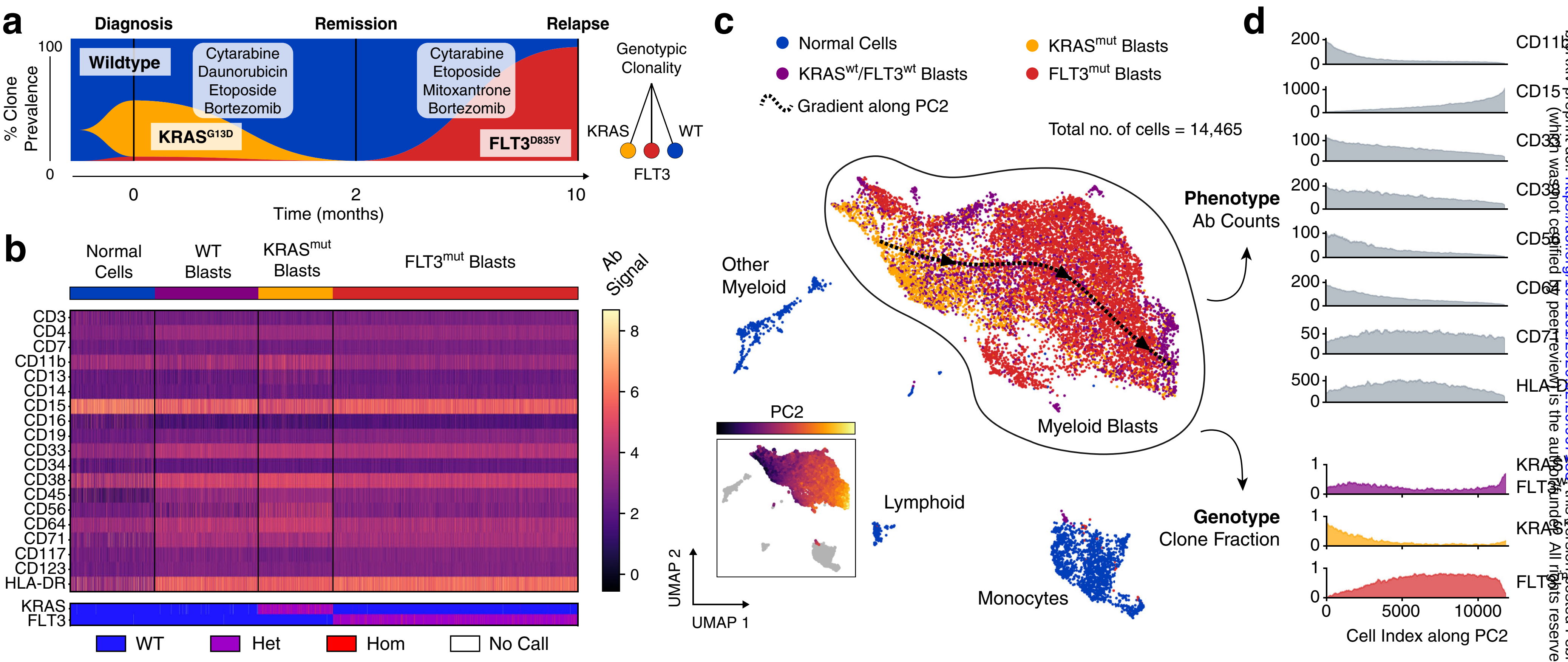

Figure 4: Distinct genetic subclones form an overlapping immunophenotypic continuum in a case of pediatric AML.
a, Three timepoints sampled with DAb-seq during treatment comprise a mixture of independent clones (KRAS G13D heterozygous blasts, yellow; FLT3 D835Y blasts, red). The wildtype compartment contains additional cells with a blast-like immunophenotype lacking detectable mutations. **b**, Heatmap of log-transformed corrected antibody counts and genotyping calls for the KRAS and FLT3 loci for each cell across all timepoints. The heatmap is grouped by genotype. Cells with wildtype genotype but blast-like immunophenotype are labeled separately. **c**, UMAP embedding of all cells from all time points based on log-transformed corrected antibody counts. Color indicates mutation status as in a. The blast compartment is overlaid with a spline approximating the gradient of the 2nd principal component of the antibody count matrix (shown in inlet figure) and indicates a gradual change in immunophenotype. **d**, Moving average expression of antibodies and fraction of mutated cells sorted by the 2nd principal component of the antibody count matrix. The overlapping phenotypic continuum between the genetically distinct blast clones is apparent.

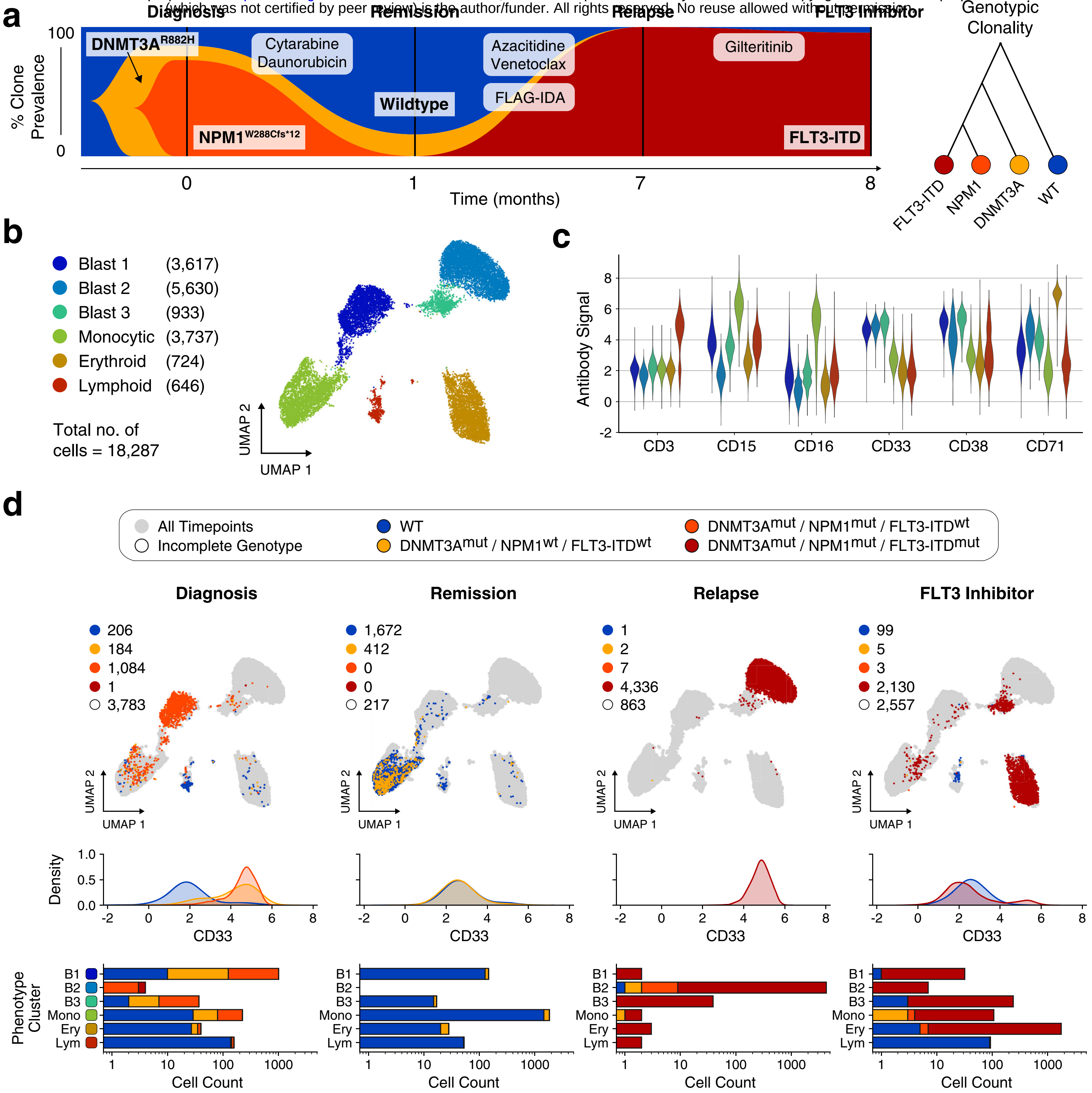

Figure 5: Decoupling of blast phenotype and genotype in response to FLT3 inhibitor therapy.

a, Fishplot showing observed fraction of cells with distinct genetic mutations for each sampled time point. The co-occurrence of the three mutations in the single-cell data is consistent with a linear model of mutation accumulation. **b**, UMAP embedding of all cells based on measured antibody signal. The cells segregate into six distinct phenotypic clusters with multiple blast compartments. **c**, Average expression of each cell cluster for a selection of markers. **d**, Top row: Same UMAP embedding as in b given as grey outline. For each sampled time point, observed cells are plotted and colored according to the detected genotype. Blasts distribute among multiple phenotypic compartments in the final time point following FLT3 inhibitor treatment. Middle row: Kernel density plot of the CD33 antibody signal resolved by time point and genotype. Cells from genotypic compartments with less than 10 cells per time point are not plotted. Bottom row: Bar chart depicting genotypic composition of each phenotypic cluster in b resolved by time point.

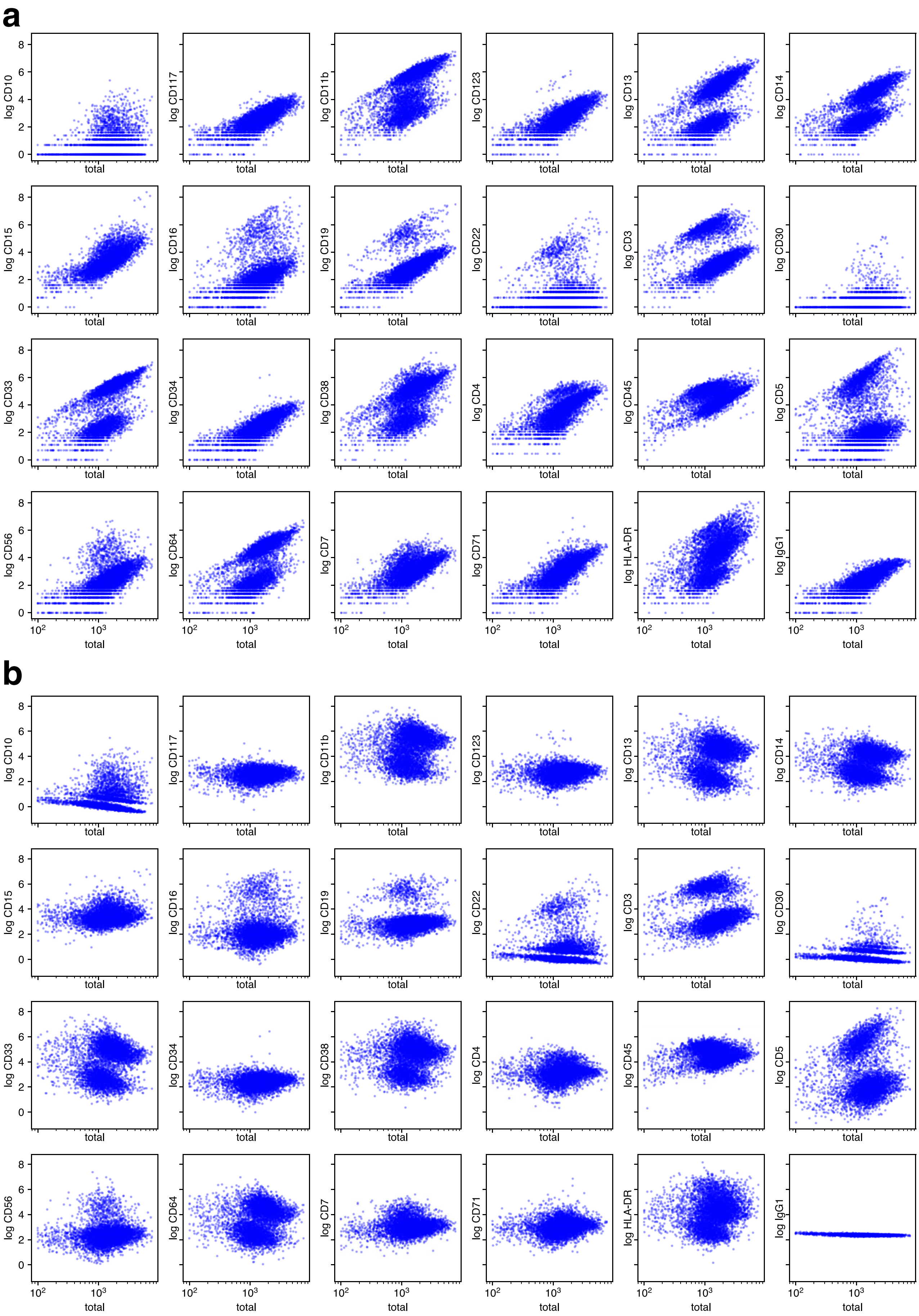

Extended Data Figure 1: Antibody count bias correction by linear regression.
a, Raw UMI counts for each antibody and cell are plotted versus total antibody count from the same cell. A clear correlation between the two is visible. A similar slope is visible for the isotype control (bottom row, rightmost column), suggesting technical bias. **b**, Same plots as in a after correcting for global droplet performance by linear regression (see Methods). Correlation with total antibody counts is reduced.